

DOI: [10.29026/oea.2025.240109](https://doi.org/10.29026/oea.2025.240109)CSTR: [322.47.14.oea.2025.240109](https://cstr.net/urn:cstr:322.47.14.oea.2025.240109)

Smart reconfigurable metadevices made of shape memory alloy metamaterials

Shiqiang Zhao^{1,2}, Yuancheng Fan^{1*}, Ruisheng Yang¹, Zhehao Ye¹,
Fuli Zhang^{1*}, Chen Wang², Weijia Luo², Yongzheng Wen^{2*} and Ji Zhou^{2*}

¹MOE Key Laboratory of Material Physics and Chemistry under Extraordinary Conditions, School of Physical Science and Technology, Northwestern Polytechnical University, Xi'an, 710129 China; ²State Key Lab of New Ceramics and Fine Processing, Department of Materials Science and Engineering, Tsinghua University, Beijing, 100084 China.

*Correspondence: YC Fan, E-mail: phyfan@nwpu.edu.cn; FL Zhang, E-mail: fuli.zhang@nwpu.edu.cn;

YZ Wen, E-mail: wenzheng@tsinghua.edu.cn; J Zhou, E-mail: zhouji@tsinghua.edu.cn

This file includes:

[Section 1: The principle of SMA](#)

[Section 2: The geometry parameters of the designed metadevice](#)

[Section 3: The simulation setting](#)

[Section 4: The experimental setup and absorption value of metadevice](#)

[Section 5: Trapped mode for long stick metadevice](#)

[Section 6: The parameters of dual-band metadevice](#)

Supplementary information for this paper is available at <https://doi.org/10.29026/oea.2025.240109>



Open Access This article is licensed under a Creative Commons Attribution 4.0 International License.

To view a copy of this license, visit <http://creativecommons.org/licenses/by/4.0/>.

© The Author(s) 2025. Published by Institute of Optics and Electronics, Chinese Academy of Sciences.

Section 1: The principle of SMA

Shape memory alloy (SMA) is a type of temperature phase transition material with excellent performance, which can be dated back to 1932^{S1}. The shape memory effect (SME) gained wide attention when W. J. Buehler found that the Ti-Ni alloy, with an equal atomic ratio, could be restored to the morphology of the parent phase after being heated^{S2}. In this work, we use Ti-Ni SMA with thermoelastic martensitic phase transition. There are four characteristic temperature points: start temperature (A_s), finish temperature (A_f) of austenite (parent phase) transformation, start temperature (M_s), finish temperature (M_f) of martensite transformation during the phase transition. The parent phase begins to transform into martensite when the temperature is below the point M_s , if stress is applied below the point M_f , twin deformation occurs in the martensite variants, and the martensite in the favorable orientation preferentially grows and generates strain. The strain remains after unloading the stress, causing the macro shape to deform. However, the stress applied should not be too large, otherwise plastic deformation will occur. When the temperature rises above point A_s , following the aforementioned process, due to the reversibility of crystallography, the martensitic phase will reverse transform along the original shear path, returning to the lattice orientation of the parent phase, thus restoring the macroscopic shape of the parent phase, exhibiting the characteristics of SME.

Figure S1(a) demonstrates the commercial SMA used in this work. To prevent damage to the SME of SMA from processing temperatures, we implemented a heat treatment process after completing the sample fabrication. The SMA samples were placed in a muffle furnace with an air atmosphere at 500 °C for an hour. Subsequently, the furnace was turned off, and after four hours, the samples were cooled to 200 °C before being removed and allowed to air-cool to room temperature. We used differential scanning calorimetry analyzer with temperature change rate of 5 °C/min to observe its phase transition behavior between 0 and 90 °C, identifying four characteristic temperatures with values of $M_s=52$ °C, $M_f=32$ °C, $A_s=40$ °C, $A_f=76$ °C (as illustrated in Fig. S1(b)). Phase transitions occur during the heating and cooling stage, respectively. The peaks at 0 °C and 90 °C are thermal artifacts caused by the instrument and are independent of the phase transition. We experimentally measured the recovery rate, defined as the ratio of the deformation angle θ of the metadvice in Figure S1(c) to the time required for it to return to zero, to determine the appropriate heating temperature for subsequent experiments. The experimental setup for the recovery rate test is shown in the inset of Fig. S1(d). We use a temperature-controlled heating box to heat the metadvice, causing it to deform, and then use a timer to record the time, thereby obtaining the recovery rate. Figure S1(d) shows that the recovery rate rises rapidly as the heating temperature increases with a constant maximum of 91%/s. The martensite phase has been completely transformed

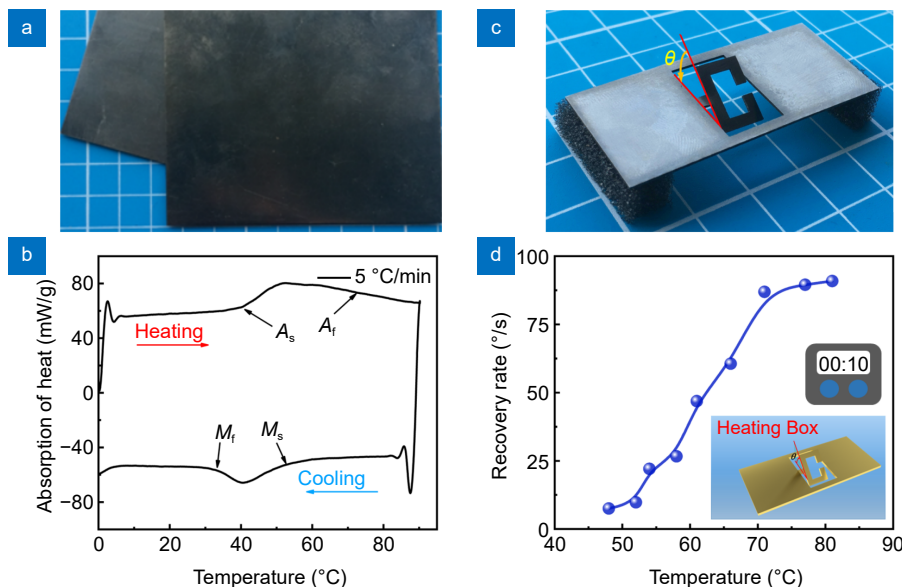


Fig. S1 | Schematic and the characteristic response to temperature of SMA. (a) SMA thin sheet after heat treatment with 0.5 mm thickness. (b) Differential scanning calorimetry curve of SMA. We can obtain four characteristic temperature points: A_s , A_f , M_s , M_f . (c) Illustration of deformed angle recovery of device processed. (d) Results of average recovery rate under testing at a series of heating temperatures.

into austenite phase after the temperature is higher than A_f . We selected the experimental recovery temperature T_H as 55 °C to fulfill our measurements, and low temperature $T_L = 25$ °C to ensure the SMA is entirely in the martensite phase without heating.

Section 2: The geometry parameters of the designed metadvice

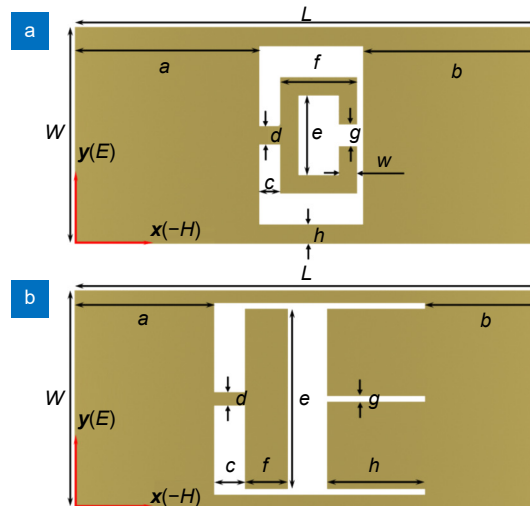


Fig. S2 | Illustration of two metadvice designed. (a) The schematic and description of geometrical parameters of SRR structure, where $L=47.55$ mm, $W=22.15$ mm, $a=18.875$ mm, $b=18.095$ mm, $c=2.1$ mm, $d=1.9$ mm, $e=8.1$ mm, $f=7.9$ mm, $g=2.2$ mm, $h=1.995$ mm, $w=1.9$ mm, and metal thickness $t=0.5$ mm. (b) The schematic and parameters of long stick structure, where $a=14.275$ mm, $b=11.775$ mm, $c=3.12$ mm, $d=1.4$ mm, $e=18.4$ mm, $f=4.4$ mm, $g=0.55$ mm, $h=10$ mm, the remaining parameters are consistent with the SRR structure in (a).

Section 3: The simulation setting

As shown in the [Figure S3](#), we utilized the finite difference time domain (FDTD) method to simulate the electromagnetic response of the designed metadvice. The simulation frequency range was set from 4 to 6 GHz. The simulation environment was configured as a waveguide environment, with corresponding boundary conditions: electric boundaries along the x and y directions, and open boundaries along the z direction. For the free space environment simulation, we used an incident y -polarized plane wave propagating along the z -direction, while setting periodic boundary conditions in the x - y directions to simulate the metasurface.

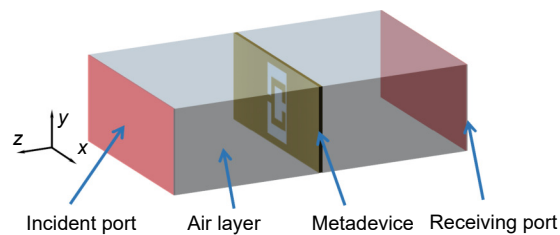


Fig. S3 | The illustration of the simulation setup.

In the simulation, the SMA was defined as a lossy metallic material with a conductivity of 1×10^6 S/m, and a thickness of 0.5 mm. The angle θ between the metamaterial resonant structure and the metal plane was set as a variable in the simulation. Based on the data from the reference^{S3}, the resistivity range of the Ti-Ni SMA used is from 70 to 130 $\mu\Omega\cdot\text{cm}$. Therefore, we simulated the effect of changes in material resistivity on the transmission. We selected four resistivity values: 70, 90, 110, and 130 $\mu\Omega\cdot\text{cm}$, corresponding to conductivity: 1.43×10^6 , 1.11×10^6 , 0.91×10^6 and 0.77×10^6 S/m. [Figure S4](#) shows the transmission variations of the SSR-based metadvice. It can be observed that changes in resistivity do not alter the device's operating frequency; however, the increased losses result in a slight decrease in transmission. This suggests that selecting shape memory alloy materials with high conductivity can help improve transmission.

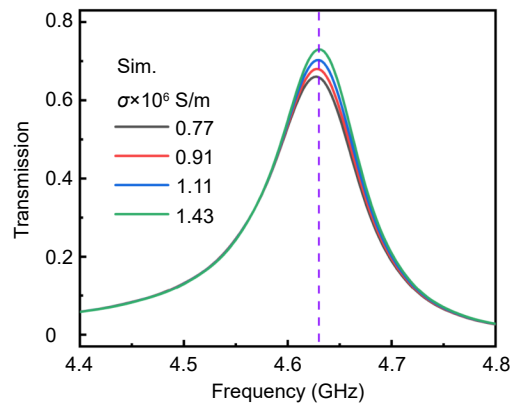


Fig. S4 | Dependence of transmission on material conductivity for SRR-based metadvice.

Section 4: The experimental setup and absorption value of metadvice

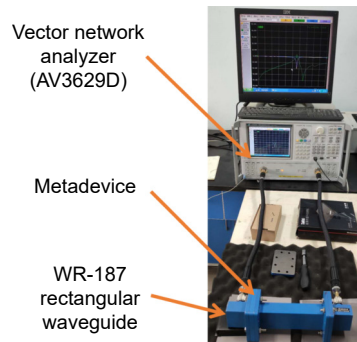


Fig. S5 | The experimental setup: we conducted experimental characterization of the designed metadvice using a waveguide. By heating the metadvice with a temperature-controlled heating box to induce deformation, we were able to measure its deformation angle θ .

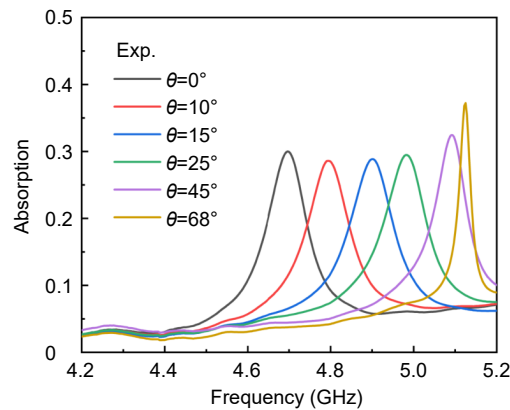


Fig. S6 | The absorption of SRR model versus angle and frequency. The absorption comes from the ohmic impedance of the metal, and reach maximum value at resonance frequency due to the maximum surface current.

Section 5: Trapped mode for long stick metadvice

We can observe that the transmission anomaly decreases at the frequency where trapped mode occurs, corresponding to an absorption extremum in [Figure S7](#).

As shown in [Fig. S8\(a\)](#), I and III are the normal transmission resonance mode, and II is the trapped mode. [Figure S8\(b\)](#) shows the surface current distributions at resonance frequency for I, II and III, the red arrows represent the direction of the currents.

It can be observed that on the metal strip, dipole oscillations form along the polarization direction of the incident

electric field, with modes I and III exhibiting relatively strong coupling with the incident field. At 5.25 GHz, two opposing dipole oscillations form on the upper and lower halves of the metal strip, causing trapped mode II to weaken in coupling with the external field, resulting in a transmission spectrum trough. Enhanced surface currents lead to strong absorption at trapped mode II. The emergence of trapped modes is induced by the configuration of the metadvice, which induces the appearance of two opposing dipoles. Figures S8(c) and d respectively show the phase of surface currents and the distribution of the electric fields. It is evident that at trapped mode II, the phase on the metal strip is in an opposite state. These analyses reveal that dipole oscillations between modes II and I, III are distinct, consistent with previous conclusions.

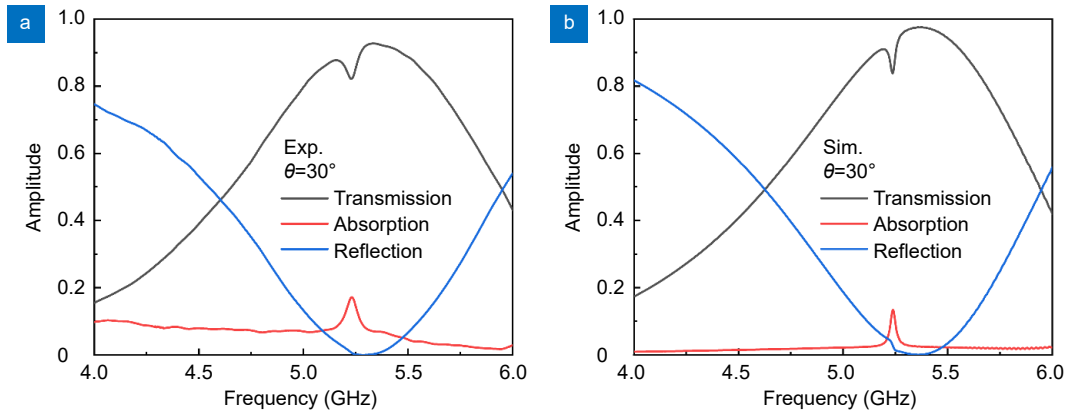


Fig. S7 | Transmission, reflection and absorption for $\theta = 30^\circ$ in long stick model.

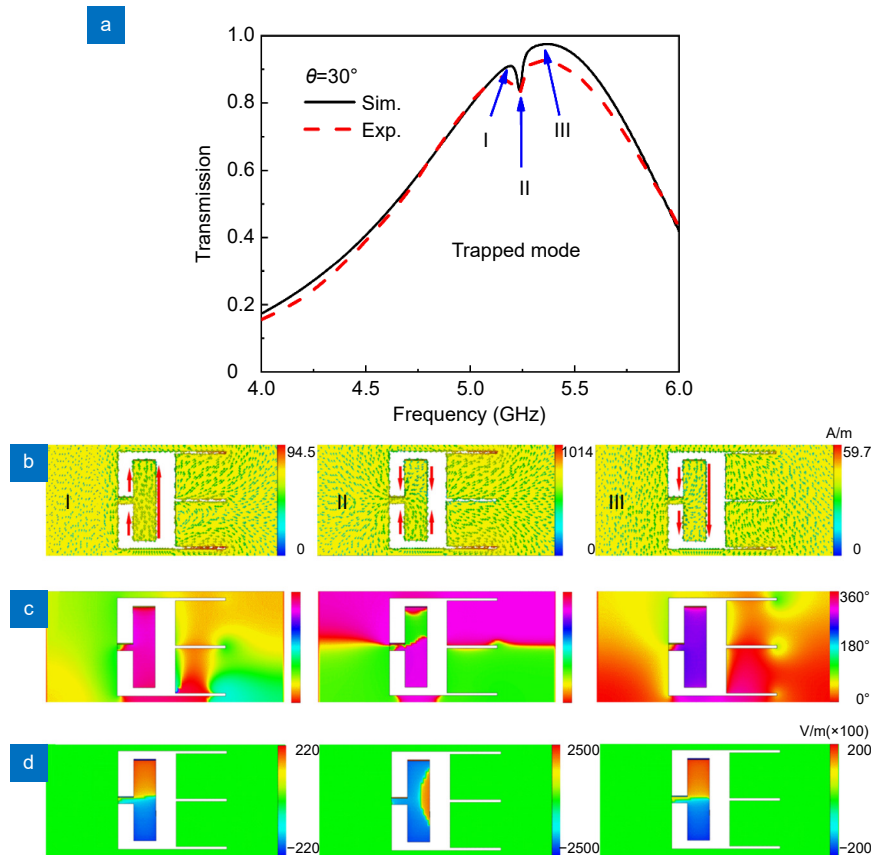


Fig. S8 | (a) Transmission spectrum for I, II and III mode at $\theta = 30^\circ$. (b) The oscillating surface current distributions. (c) Phase of surface currents and (d) the electric field distributions.

Section 6: The parameters of dual-band metadvice

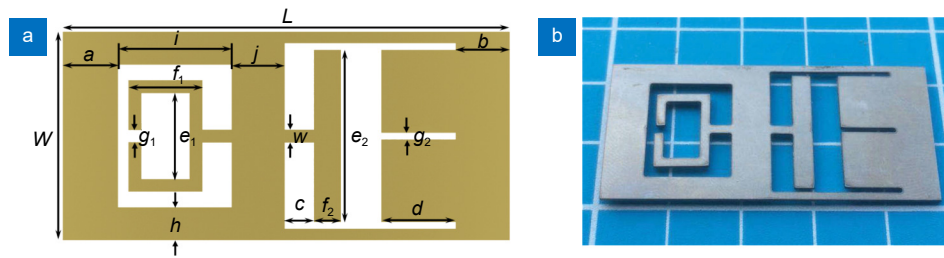


Fig. S9 | (a) Simulation model and (b) experimental sample made of SMA. where $L=47.55$ mm, $W=22.15$ mm, $a=5.9$ mm, $b=5.775$ mm, $c=3.08$ mm, $d=7.9$ mm, $e_1=9.08$ mm, $e_2=18.3$ mm, $f_1=7.9$ mm, $f_2=2.9$ mm, $g_1=1.26$ mm, $g_2=0.665$ mm, $h=3.515$ mm, $w=1.4$ mm, $i=12.06$ mm, $j=5.665$ mm.

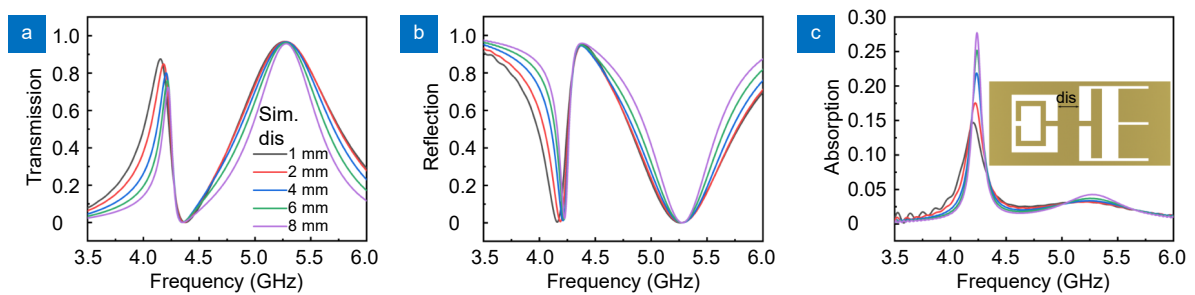


Fig. S10 | The impact of the distance between two elements on (a) transmission, (b) reflection and (c) absorption.

References

- S1. Ölander A. An electrochemical investigation of solid cadmium-gold alloys. *J Am Chem Soc* **54**, 3819–3833 (1932).
- S2. Buehler WJ, Gilfrich JV, Wiley RC. Effect of low - temperature phase changes on the mechanical properties of alloys near composition TiNi. *J Appl Phys* **34**, 1475–1477 (1963).
- S3. Wu SK, Lin HC, Lin TY. Electrical resistivity of Ti–Ni binary and Ti–Ni–X (X = Fe, Cu) ternary shape memory alloys. *Mater Sci Eng A* **438–440**, 536–539 (2006).